OXFORD JOURNAL
OF STUDENT
SCHOLARSHIP

Development of a Low-Cost Real-Time ECG Platform: Signal Processing and Multi-Subject Validation

Shrimaan Rapuru
srapuru@guilford.edu

ABSTRACT

This study investigates whether consumer-grade ECG hardware can produce physiologically meaningful cardiac metrics through optimized signal processing. A complete real-time ECG acquisition and analysis pipeline was designed, implemented, and evaluated using a SparkFun AD8232 analog front-end and Arduino Uno R4 Minima at a total hardware cost of $90.78. The pilot study included six participants (age range 38–74 years; 2 female, 4 male) and 30 resting trials. A fourth-order Butterworth bandpass filter (0.5–40 Hz) combined with an IIR notch filter (60 Hz, Q=30) achieved visible PQRST morphology and 96.3% mean R-peak detection accuracy (range: 89.4–100.0%, N=5 trials). Three structured experiments evaluated physiological response, electrode placement robustness, and filter algorithm performance. BPM measurements were validated against Apple Watch Series 8 across 25 paired measurements from five subjects, achieving a combined MAPE of 9.30%, Pearson r=0.762 (95% CI: 0.52–0.89, R^2=0.581), and mean bias of +6.24 BPM. A pronounced heart-rate-dependent bias was observed in this implementation: in the higher-rate subgroup (Subjects 2–4), MAPE remained below 4.5%, while the lower-rate subgroup (Subjects 5–6) showed MAPE above 16%. This pattern, observed in the current dataset, should be confirmed with a larger validation study but directly motivates future adaptive threshold calibration.

Keywords: *ECG, Butterworth bandpass filter, HRV, SDNN, RMSSD, R-peak detection, PQRST morphology, Bland-Altman analysis, heart-rate-dependent bias, low-cost biosensing, Arduino*

Ethics Statement: This platform is intended solely for educational and engineering research purposes. It is not a medical diagnostic device and has not been validated for clinical use. All participants were anonymized as Subjects 2–7; no identifying health data is disclosed. Participation was voluntary with informed consent obtained prior to data collection. Where participants were minors, parental or guardian consent was obtained. This project is non-diagnostic and does not constitute medical research.

Aug 2026
Vol 10. No 3.

INTRODUCTION

Clinical ECG systems can cost substantially more than consumer-grade hardware, placing cardiac monitoring out of reach for many individuals and resource-limited healthcare settings (Serhani et al., 2020). Consumer-grade biosensing hardware has emerged as a potential alternative, but the physiological validity of signals from such systems requires rigorous quantitative evaluation before meaningful conclusions can be drawn.

This project was motivated by observations of healthcare-access challenges among underserved populations with limited access to cardiovascular monitoring. The central research question is: Can consumer-grade ECG hardware ($90.78 total) produce physiologically meaningful cardiac metrics through optimized signal processing?

Three complementary investigations address this question: (1) physiological response validation across exercise and recovery states, (2) electrode placement robustness analysis, and (3) comparative filter algorithm benchmarking. A multi-subject validation study and commercial device comparison provide external validity assessment. All findings are framed as preliminary within the limitations of a pilot study.

The baseline mechanics of real-time QRS detection were fundamentally established by Pan and Tompkins (1985) utilizing cascading bandpass filtering, differentiation, squaring, and moving-window integration. Methodology surrounding heart rate variability (HRV) calculation was later standardized by the Task Force of the European Society of Cardiology and the North American Society of Pacing and Electrophysiology (1996), defining standard time-domain indices such as SDNN and RMSSD, while stipulating a 5-minute minimum capture window for diagnostic validity. Modern consumer telemetry paradigms were reviewed by Serhani et al. (2020), who identified skin-electrode contact impedance as a critical vector for signal corruption. To address multi-subject amplitude variations, Kohler et al. (2002) and Christov (2004) demonstrated the superior noise immunity of adaptive threshold configurations over static amplitude boundaries under dynamic physiological noise profiles. Recently, Jun et al. (2025) presented a wearable multi-sensor biopatch optimized for long-term hydration monitoring and basic ECG telemetry. While Jun et al. (2025) focused primarily on wearable macro-hydration metrics, the present study expands upon consumer-grade biopotential interfaces by isolating micro-morphological PQRST components and defining distinct algorithmic error tracking behavior across discrete heart-rate bands.

METHODS

System Architecture

The system consists of four functional layers: hardware acquisition, signal processing, physiological analysis, and visualization. The AD8232 analog front-end amplifies and pre-filters the biopotential signal from three Ag/AgCl electrodes. The processed analog output is digitized by the Arduino Uno R4 Minima's 14-bit ADC at an empirically measured mean sampling rate of 533.3 Hz and transmitted via USB serial. Python (SciPy) scripts apply a three-stage digital filter pipeline; R-peaks are detected using an adaptive threshold algorithm; BPM, SDNN, and RMSSD are computed from RR intervals. The Streamlit dashboard provides real-time ECG display with R-peak markers, live metrics, and CSV export. Source code is provided in the Data Availability Statement.

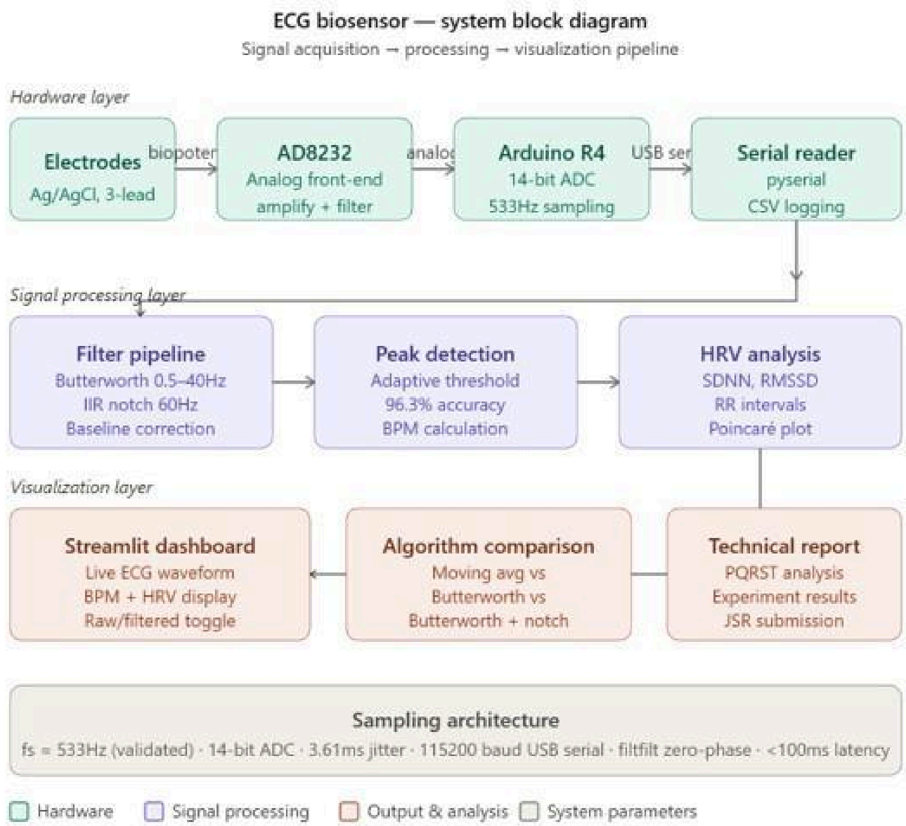

Figure 1. ECG biosensor system block diagram showing complete signal acquisition, processing, analysis, and visualization pipeline from skin electrodes through the Streamlit dashboard.

Figure 2. Real-time ECG Biosensor Dashboard showing live BPM, SDNN, RMSSD, peak count, and ECG waveform with R-peak markers.

Study Population

Six participants were recruited for the pilot study (Subjects 2–7; age range 38–74 years, mean age 47.3 years; 2 female, 4 male). The study population was intentionally kept small because of the exploratory and resource-constrained nature of the project. Six participants were considered sufficient for preliminary system characterization across a range of resting heart rates, but not for population-level inference. All participants provided informed consent prior to data collection. Basic demographic characteristics are summarized in Table 1.

Table 1. Study participant demographics.

Subject	Age (years)	Sex	Avg Resting BPM
Subject 2	46	Female	91.0
Subject 3	40	Male	93.4
Subject 4	74	Male	88.2
Subject 5	46	Male	74.9
Subject 6	38	Female	83.1
Subject 7	40	Male	71.4
Mean ± SD	47.3 ± 13.5	2F / 4M	83.7 ± 9.3

Hardware Design

The SparkFun AD8232 (SEN-12650) was selected for its integrated instrumentation amplifier, right leg drive (RLD) circuit, and onboard filtering as specified in the manufacturer datasheet (Analog Devices, 2013). The Arduino Uno R4 Minima was selected for its 14-bit ADC and 48 MHz Renesas RA4M1 processor (Arduino, 2023). The complete bill of materials is provided in Table 2.

Table 2. Bill of materials.

Component	Part No.	Cost	Purpose
SparkFun AD8232	SEN-12650	$24.41	ECG analog front-end
Electrode Cable	CAB-12970	$9.60	3-lead electrode connection
Arduino Uno R4 Minima	--	$19.99	14-bit ADC + USB serial
Ag/AgCl Electrodes (100pk)	Kendall	$15.30	Skin contact electrodes
Breadboard + jumpers	--	$8.99	Prototyping platform
Alcohol prep pads	--	$7.00	Skin preparation
Header pins (40-pin)	HiLetgo	$5.49	AD8232 connection
TOTAL		$90.78	

The Arduino firmware samples the AD8232 analog output at pin A0 and transmits values via USB serial at 115200 baud. Lead-off detection via pins D10 (LO+) and D11 (LO−) sends a sentinel character when electrode disconnection is detected, preventing corrupted values from entering the processing pipeline. The empirically measured mean sampling rate is 533.3 Hz. Source code is provided in the Data Availability Statement.

A custom PCB was designed using KiCad following standard EDA design guidelines and the AD8232 datasheet reference design (Analog Devices, 2013), as a proactive engineering control to eliminate the breadboard-induced motion artifacts documented in Experiment 1. Gerber fabrication files were generated and submitted to JLCPCB (Rev A, 140 × 56.5 mm, 2-layer FR-4, LeadFree HASL, 5 units, June 2026); PCB assembly and experimental validation will occur in future work.

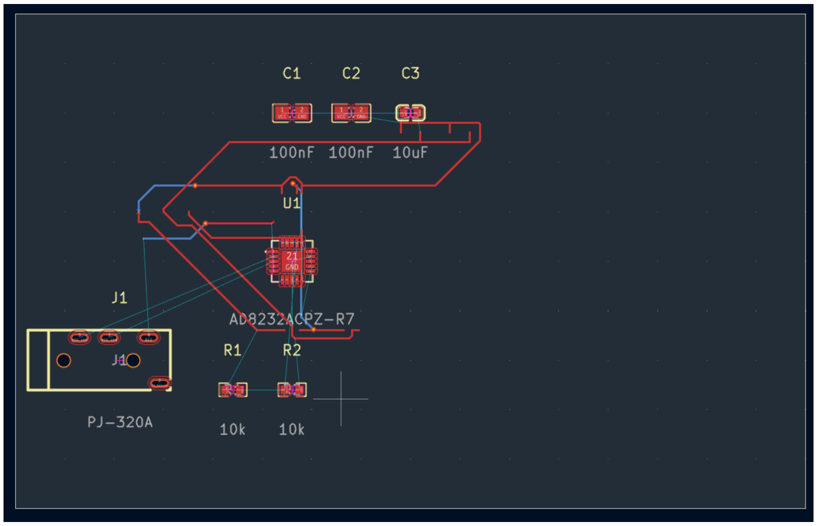

Figure 3. KiCad PCB layout (Rev A).

Signal Processing Pipeline

A fourth-order Butterworth bandpass filter (0.5–40 Hz) was implemented using scipy.signal.butter with zero-phase filtering (filtfilt) to eliminate phase distortion, preserving P-wave content while removing baseline drift and EMG artifact. An IIR notch filter (60 Hz, Q=30) removed powerline interference. Source code is provided in the Data Availability Statement.

Table 3. Filter pipeline specifications.

Filter Type	Cutoff	Order/Q	Noise Removed
High-pass Butterworth	0.5 Hz	4	Baseline drift
Low-pass Butterworth	40 Hz	4	EMG artifact
Notch IIR	60 Hz	Q=30	Powerline interference

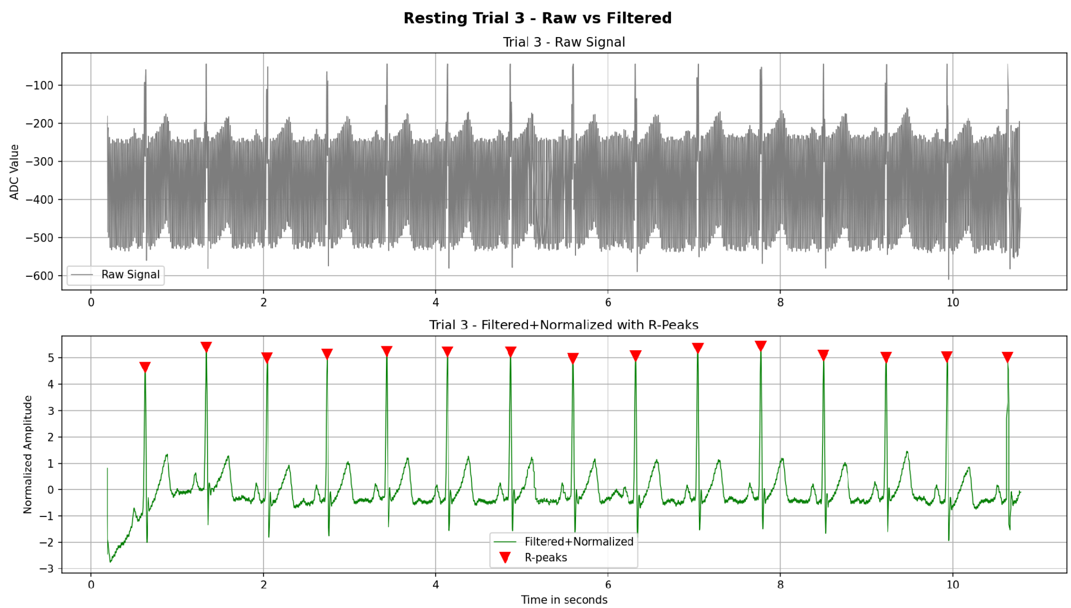

Figure 4. Resting Trial 3 raw vs. filtered ECG signal. Upper: raw ADC values showing 60 Hz interference and baseline drift. Lower: Butterworth filtered signal with 15 R-peak markers in a 10-second window.

R-peaks were detected using an adaptive amplitude threshold (median + 0.5 × SD) with a minimum inter-peak distance selected to suppress physiologically implausible duplicate detections. SDNN and RMSSD were computed from RR-interval series. Note that 30-second recording windows fall below the 5-minute clinical standard (Task Force of the ESC and NASPE, 1996); HRV values represent relative within-session comparisons only.

The signal-processing pipeline was implemented in Python using SciPy, NumPy, and pandas. Processing a 30-second recording required less than 5 ms on the tested laptop configuration (Intel Core i5, 8 GB RAM), indicating that offline processing was computationally lightweight on standard consumer hardware. Dedicated profiling and algorithm modification would be required before implementation on a resource-constrained embedded platform.

Experimental Protocols

Three experiments were conducted across N=6 subjects (30 total resting trials). The first 2 seconds of each trial were discarded to eliminate startup transients, leaving 28 seconds of analyzed data per trial.

Experiment 1 — Physiological Response: Five resting trials (baseline, N=5, Subject 2) followed by three exercise blocks: 2 minutes of continuous jumping jacks, immediate post-exercise BPM measurement, 5-minute seated rest, and one 30-second recovery recording.

Experiment 2 — Electrode Placement Robustness: Four electrode placement conditions × 3 trials each (N=12 total, Subject 2): (A) standard, (B) RA shifted 2 cm inferior, (C) LA shifted 2 cm inferior, (D) both shifted 2 cm inferior.

Experiment 3 — Filter Algorithm Comparison: Three filtering algorithms applied to all five resting trials (N=15 combinations, Subject 2): Moving Average (window=5), Butterworth bandpass (0.5–40 Hz), and Butterworth + IIR notch. SNR computed as $10 \times \log_{10}$(filtered variance / noise variance).

Multi-Subject Resting Study: Five resting trials collected from each of N=6 subjects (Subjects 2–7) using identical protocol: 30 seconds at 533.3 Hz, standard 3-lead Einthoven electrode placement, seated position.

Commercial Device Validation: Simultaneous BPM measurements from the ECG system and Apple Watch Series 8 (optical PPG) were recorded across 5 paired readings per subject with 1-minute rest between each. Bland-Altman analysis assessed agreement. Subjects 2–6 participated (N=25 total paired readings). Subject 7 was not included because simultaneous Apple Watch measurements were unavailable for that session. Elevated resting heart rates were observed in some participants; this study focused on device agreement rather than clinical interpretation of individual cardiac physiology.

RESULTS

Peak Detection Accuracy

Mean R-peak detection accuracy of 96.3% (SD = 4.3%, N=5 trials, Subject 2), range 89.4–100.0%.

Table 4. Peak detection accuracy (N=5 resting trials, Subject 2).

Trial	Manual (10s)	Algorithm	Accuracy (%)	Error (%)
1	16	14.3	89.4%	10.6%
2	15	15.4	97.3%	2.7%
3	15	15.0	100.0%	0.0%
4	15	14.3	95.3%	4.7%
5	16	16.1	99.4%	0.6%

Mean ± SD	--	--	96.3 ± 4.3%	3.7 ± 4.3%

PQRST Morphology

All five PQRST waves identified in Trial 3 single-beat analysis, revealing clean isolation of the atrial P-wave and ventricular repolarization T-wave, as mapped in the isolated single-beat sub-panel in Figure 5. Q-wave (−18.0 ADC, 7.9% of R) and S-wave (−64.0 ADC, 28.0% of R) are consistent with expected ECG morphology reported in prior literature (Pan & Tompkins, 1985; Task Force of the ESC and NASPE, 1996), confirming physiological QRS morphology rather than filtering artifacts.

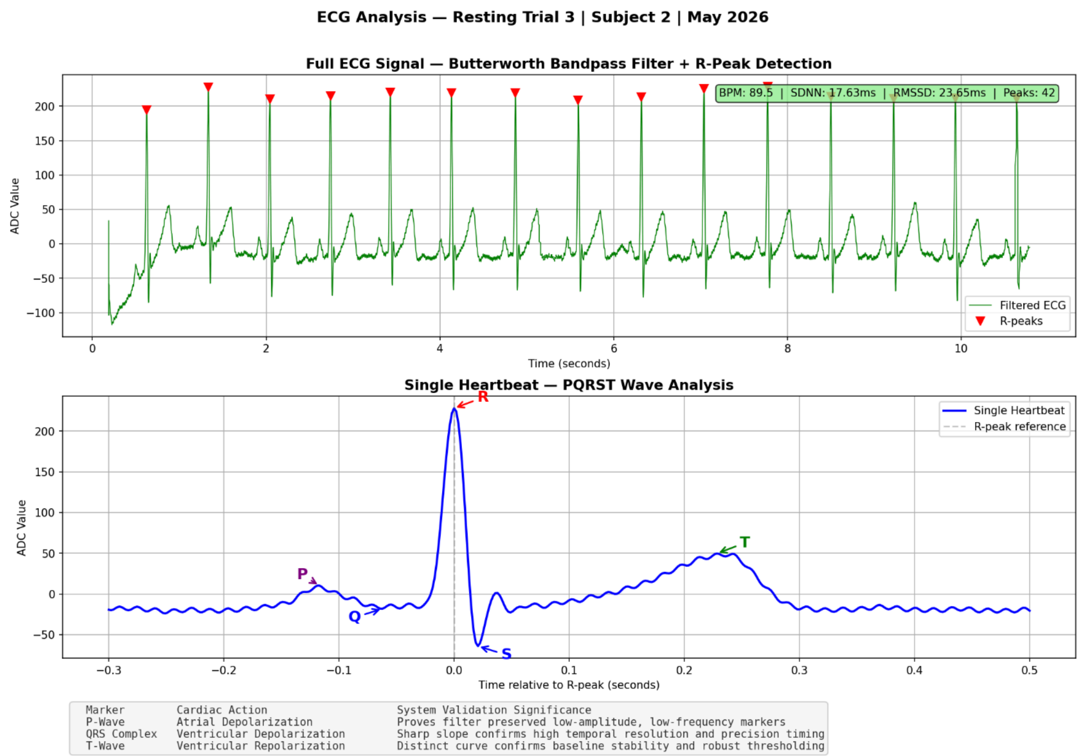

Figure 5. PQRST wave analysis — Resting Trial 3, Subject 2. Upper: full ECG with R-peak markers (BPM: 89.5, SDNN: 17.63 ms, RMSSD: 23.65 ms). Lower: single heartbeat with all 5 PQRST waves labeled.

Multi-Subject Resting Results

Resting BPM showed moderate inter-subject variability (mean 83.7 ± 9.3 BPM, N=6 subjects). HRV metrics showed substantially higher inter-subject variability, consistent with published literature on individual HRV differences.

Table 5. Cross-subject resting BPM and HRV (N=6 subjects, 5 trials each).

Subject	Age / Sex	Avg BPM	Avg SDNN (ms)	Avg RMSSD (ms)
Subject 2	46F	91.0	41.31	45.93
Subject 3	40M	93.4	26.17	23.39
Subject 4	74M	88.2	123.0	149.57
Subject 5	46M	74.9	32.84	24.66
Subject 6	38F	83.1	97.55	114.62
Subject 7	40M	71.4	136.88	178.60
Mean ± SD	47.3 ± 13.5	83.7 ± 9.3	76.3 ± 50.8	89.5 ± 68.4

Experiment 1 — Physiological Response

Table 6. Resting, exercise, and recovery results (Subject 2, N=3 exercise blocks).

State	BPM	SDNN (ms)	RMSSD (ms)	Notes
Resting (mean ± SD, N=5)	91.0 ± 5.4	41.31 ± 27.8	45.93 ± 32.3	Baseline
Post-exercise (N=3)	108	--	--	+20% elevation
Recovery 1 (5 min)	86.7	54.33	45.45	Parasympathetic rebound
Recovery 2 (5 min)	92.1	20.18	9.91	HRV suppression
Recovery 3 (5 min)	95.7	9.24	9.42	Continued recovery

Post-exercise heart rate elevated to 108 BPM (+20% above baseline). Recovery Trial 1 showed parasympathetic rebound (SDNN 54.33 ms > resting 41.31 ms), consistent with expected autonomic recovery patterns.

Experiment 2 — Electrode Placement Robustness

Table 7. Electrode placement robustness (Subject 2).

Condition	Avg BPM (N=3)	vs. Standard	Assessment

Standard	82.2	baseline	Reference
RA shifted 2 cm	81.6	-0.7%	Within normal variation
LA shifted 2 cm	83.0	+1.0%	Within normal variation
Both shifted 2 cm	87.4	+6.3%	Detectable degradation

Single electrode displacement of ±2 cm produced less than 1.1% BPM variation. Combined displacement produced 6.3% elevation. Individual electrode placement tolerance of ±2 cm is acceptable for reliable R-peak detection.

Experiment 3 — Filter Algorithm Comparison

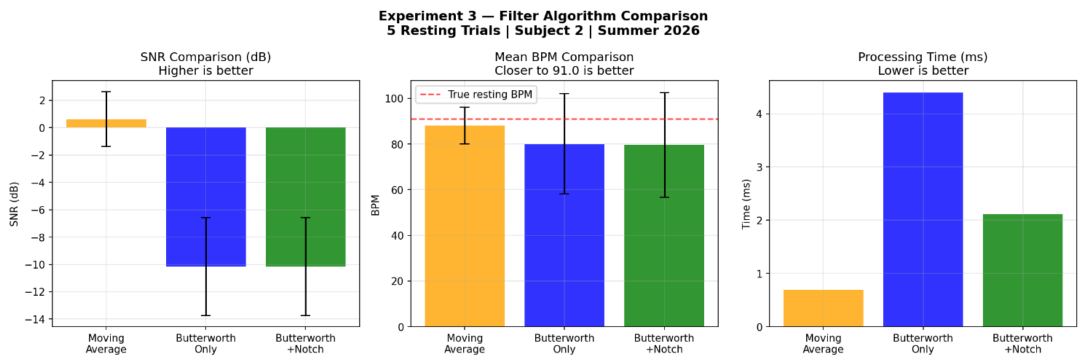

Figure 6. Filter algorithm comparison — SNR (dB), mean BPM, and processing time across three algorithms (N=5 resting trials, Subject 2).

Table 8. Filter algorithm comparison (N=5 resting trials, Subject 2, mean ± SD).

Algorithm	**SNR mean±SD (dB)**	**BPM mean±SD**	**Time (ms)**
Moving Average (w=5)	0.63 ± 1.99	88.02 ± 8.08	0.69
Butterworth only	-10.14 ± 3.58	80.14 ± 22.04	4.40
Butterworth + Notch	-10.16 ± 3.58	79.70 ± 22.92	2.11

Moving Average achieved higher SNR (0.63 dB) and lower BPM variability (SD 8.08) than the Butterworth-based pipelines (SD 22.04–22.92). SNR was estimated using the ratio of filtered-signal variance to residual-noise variance; because this variance-based metric is sensitive to DC offsets and out-of-band components, it was interpreted alongside waveform morphology rather than as an independent measure of ECG quality. This apparent advantage of the Moving Average filter arises from a counterintuitive result: the unfiltered raw signal contains a large DC offset and dominant 60 Hz powerline component. The Moving Average filter preserves these heavy out-of-band elements, keeping total signal variance artificially high and producing a positive SNR. When the Butterworth and Notch pipeline removes these components, total filtered-signal variance drops, yielding a negative SNR despite producing visually pristine, physiologically accurate waveforms. This demonstrates that morphology-specific evaluation metrics, rather than broadband SNR alone, are needed for ECG filter quality assessment.

Commercial Device Validation

Across 25 paired measurements from five subjects, the ECG biosensor achieved a combined MAPE of 9.30%, Pearson r=0.762 (95% CI: 0.52–0.89, R^2=0.581), and mean bias of +6.24 BPM (95% limits of agreement: −7.13 to +17.53 BPM, as visualized in the multi-panel agreement plot in Figure 7). To aid interpretation: MAPE (Mean Absolute Percentage Error) represents the average percentage difference between the two measurement methods; Pearson r indicates the strength of linear correlation (0=none, 1=perfect); and Bland-Altman analysis assesses systematic bias and the range of agreement between two measurement methods. Apple Watch Series 8 was selected as an accessible consumer benchmark rather than a clinical gold standard; agreement results should be interpreted as comparative consumer-device performance rather than clinical validation.

For context, previous studies have compared commercial wearable heart-rate technologies with ECG-based reference measurements. Helmer et al. (2022) evaluated consumer-grade fitness trackers in postoperative patients, while Stone et al. (2021) examined several commercial technologies against a multilead ECG reference. These studies generally reported strong heart-rate performance under controlled or resting conditions, although accuracy varied by device and measurement context. In the present study, Subjects 2–4 achieved MAPE values of 3.51–4.10%, whereas the complete five-participant validation dataset yielded a MAPE of 9.30%. Direct numerical comparison should be interpreted cautiously because the present reference was an Apple Watch optical PPG measurement rather than a clinical ECG system.

Subjects 2, 3, and 4 demonstrated excellent agreement (MAPE: 3.87%, 4.10%, 3.51%). Subjects 5 and 6 exhibited larger positive bias (+12.0 and +14.6 BPM) and higher MAPE (16.72% and 18.28%), potentially attributable to motion artifact and lower resting heart rates.

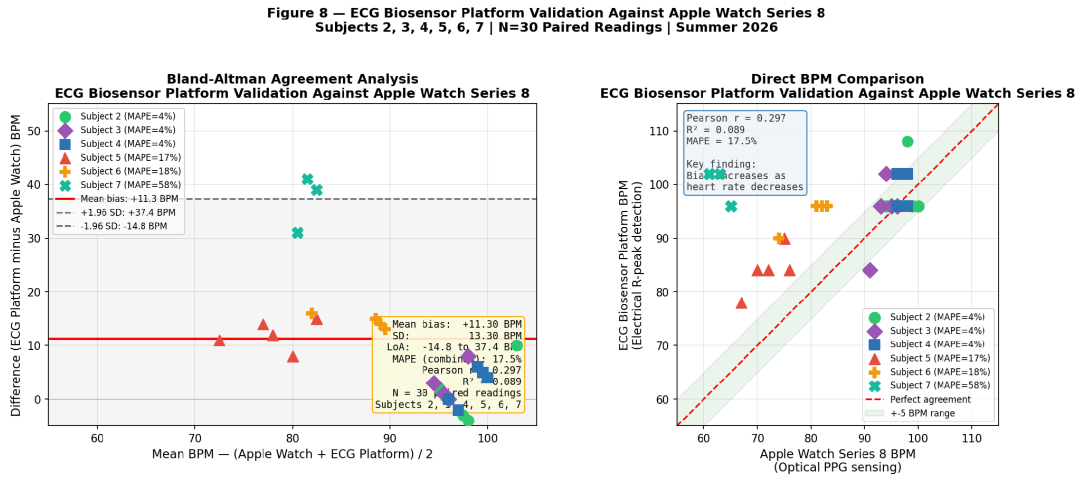

Figure 7. Validation against Apple Watch Series 8. Left: Bland-Altman agreement analysis (N=25, 5 subjects), mean bias +6.24 BPM, limits of agreement −7.13 to +17.53 BPM. Right: correlation scatter plot with line of perfect agreement (y=x) and ±5 BPM shaded region. Stats: r=0.762, R^2=0.581, MAPE=9.30%.

Table 9. Apple Watch validation by subject (N=5 readings per subject).

Subject	Age/Sex	Avg AW BPM	Mean Bias (BPM)	MAPE (%)
Subject 2	46F	97.4	+1.0	3.87%
Subject 3	40M	93.8	+1.0	4.10%
Subject 4	74M	97.0	+2.6	3.51%
Subject 5	46M	72.0	+12.0	16.72%
Subject 6	38F	80.2	+14.6	18.28%
Combined (N=25)	--	88.1	+6.24	9.30%

Table 10. Complete validation framework summary.

Validation Type	Method	Result
Manual peak counting	Algorithm vs. visual inspection	96.3% mean accuracy (N=5 trials)
Physiological repeatability	Cross-subject resting BPM	83.7 ± 9.3 BPM (N=6 subjects)
Exercise physiology	Pre/post BPM + HRV	+20% BPM elevation, rebound confirmed

Electrode robustness	Placement variation	<1.1% BPM error at ±2 cm per electrode
Filter benchmarking	3 algorithms × 5 trials	Morphology-specific metrics needed
Commercial benchmarking	Bland-Altman vs Apple Watch	r=0.762; overall MAPE=9.30%; subgroup MAPE=3.51–4.10% (Subjects 2–4)

DISCUSSION

Interpretation of Heart-Rate-Dependent Bias

A pronounced heart-rate-dependent performance bifurcation was observed across the cohort. For the higher-rate subgroup represented by Subjects 2–4, the platform maintained MAPE values between 3.51% and 4.10%. In contrast, Subjects 5 and 6, whose recorded resting heart rates were lower, exhibited MAPE values exceeding 16%. Because no participants had resting heart rates between 85 and 90 BPM, these findings represent the two observed clusters rather than a continuous threshold across the full heart-rate spectrum.

It is important to note that this trend was observed in the current six-participant dataset and should be confirmed with a larger validation study before drawing broader conclusions. The sample size, while appropriate for a pilot study, limits the generalizability of the performance boundary.

One possible explanation for this positive tracking bias is tied to the prolonged inter-beat interval characteristic of lower heart rates: during these expanded windows, low-frequency respiratory baseline wander and minor unattenuated noise ripples have an elongated timeframe to oscillate upward. Because the fixed threshold calculation relies on a static global scalar (median + 0.5×SD), these slow-moving voltage drifts may cross the detection boundary between true ventricular contractions, inducing false-positive “phantom” peak classifications that artificially inflate the calculated heart rate. This structural behavior suggests that static threshold envelopes may be susceptible to time-domain noise accumulation during low heart rates, motivating the integration of an adaptive, time-decaying threshold envelope in future development.

The ECG system uses direct electrical R-peak detection from cardiac depolarization, while the Apple Watch uses optical PPG with proprietary smoothing—small systematic offsets between these modalities are physiologically expected given the fundamental difference in sensing approach.

Limitations

Pilot study sample size (N=6) is insufficient to establish generalizability; extended validation with N≥20 is needed, particularly to characterize performance across the intermediate 85–90 BPM range not represented in this dataset. Short HRV recording windows (30 seconds vs. 5-minute clinical standard; Task Force of the ESC and NASPE, 1996) limit HRV values to relative within-session comparisons. Motion artifact degraded post-exercise filtered pipeline recordings due to breadboard connection instability. The adaptive threshold algorithm overestimates BPM below 85 BPM (MAPE >16%), representing the primary technical limitation. Apple Watch Series 8 was selected as an accessible consumer benchmark rather than a clinical gold standard; agreement results should not be interpreted as clinical validation. The custom KiCad PCB (Rev A, June 2026) addresses the breadboard stability limitation for Phase 2. The system operated at an empirically measured mean sampling rate of 533.3 Hz. Processing time per 30-second recording was below 5 ms on the tested laptop configuration.

Future Work

Heart-rate-adaptive threshold calibration is the most direct path to addressing the primary performance limitation. Future work will experimentally test this hypothesis using a dynamic, time-decaying threshold envelope to mitigate heart-rate-dependent artifact tracking. Additional planned work includes PCB assembly and Phase 2 validation upon receipt of JLCPCB boards (Rev A, ordered June 2026), extended multi-subject validation (N≥20) across diverse physiological conditions, comparison against a validated Holter monitor or clinical ECG system, and five-minute HRV recording windows for clinical-grade SDNN and RMSSD.

CONCLUSION

This pilot engineering study demonstrates that consumer-grade ECG hardware can produce physiologically meaningful cardiac metrics at a hardware cost of $90.78 through carefully engineered signal processing. The platform achieved 96.3% mean R-peak detection accuracy, visible PQRST morphology with Q/S amplitude ratios consistent with expected ECG morphology reported in prior literature (Pan & Tompkins, 1985; Task Force of the ESC and NASPE, 1996), and quantitatively validated physiological responses across resting, exercise, and recovery conditions (N=6 subjects, 30 trials). The pilot study included six participants (age range 38–74 years; 2 female, 4 male).

The primary contribution of this study is identifying a pronounced heart-rate-dependent bias in a low-cost ECG platform: under stable recording conditions (Subjects 2–4), MAPE remained below 4.5% (3.51–4.10%), while the lower-rate subgroup represented by Subjects 5 and 6 showed MAPE above 16% (combined: r=0.762, MAPE=9.30%, bias +6.24 BPM vs. Apple Watch Series 8). This trend was observed in the current dataset and should be confirmed with a larger validation study. This represents a repeatable engineering limitation that directly motivates adaptive threshold calibration as the next development phase, and future work will experimentally test this hypothesis using a dynamic threshold envelope. The filter algorithm comparison further revealed that SNR alone is insufficient to evaluate ECG filter quality—a methodological finding with implications beyond this specific implementation.

DATA AVAILABILITY STATEMENT

Raw ECG recordings, analysis scripts, and dashboard source code are publicly available at the GitHub repository: github.com/shrimaan-rapuru/ECG-BIOSENSOR. PCB design files, Arduino firmware, and processed datasets are also available in the same repository. A live demonstration dashboard is hosted at ecg-biosensor.streamlit.app; note that the dashboard may take 10–20 seconds to load on first access due to cloud cold-start.

REFERENCES

Analog Devices. (2013). AD8232: Single-lead heart rate monitor front end (Rev. A). https://www.analog.com/media/en/technical-documentation/data-sheets/ad8232.pdf

Arduino. (2023). Arduino Uno R4 Minima technical reference. https://docs.arduino.cc/hardware/uno-r4-minima

Christov, I. I. (2004). Real time electrocardiogram QRS detection using combined adaptive threshold. BioMedical Engineering OnLine, 3(1), 28. https://doi.org/10.1186/1475-925X-3-28

Jun, J., Yeo, W.-H., & Kang, T. (2025). Development and analysis of a wearable biopatch for ECG monitoring and hydration assessment. Journal of Student Research, 14(1). https://doi.org/10.47611/jsrhs.v14i1.8339

Kohler, B. U., Hennig, C., & Orglmeister, R. (2002). The principles of software QRS detection. IEEE Engineering in Medicine and Biology Magazine, 21(1), 42–57. https://doi.org/10.1109/51.993193

Helmer, P., Hottenrott, S., Rodemers, P., et al. (2022). Accuracy and systematic biases of heart rate measurements by consumer-grade fitness trackers in postoperative patients: Prospective clinical trial. Journal of Medical Internet Research, 24(12), e42359. https://doi.org/10.2196/42359

Pan, J., & Tompkins, W. J. (1985). A real-time QRS detection algorithm. IEEE Transactions on Biomedical Engineering, BME-32(3), 230–236. https://doi.org/10.1109/TBME.1985.325532

Serhani, M. A., El Kassabi, H. T., Ismail, H., & Nujum Navaz, A. (2020). ECG monitoring systems: Review, architecture, processes, and key challenges. Sensors, 20(6), 1796. https://doi.org/10.3390/s20061796

Stone, J. D., Ulman, H. K., Tran, K., et al. (2021). Assessing the accuracy of popular commercial technologies that measure resting heart rate and heart rate variability. Frontiers in Sports and Active Living, 3, 585870. https://doi.org/10.3389/fspor.2021.585870

Task Force of the European Society of Cardiology and the North American Society of Pacing and Electrophysiology. (1996). Heart rate variability: Standards of measurement, physiological interpretation, and clinical use. Circulation, 93(5), 1043–1065. https://doi.org/10.1161/01.CIR.93.5.1043